Global Biogeochemical Cycles

RESEARCH ARTICLE
10.1029/2018GB006125

Effects of Eddy-Driven Subduction on Ocean Biological Carbon Pump

Laure Resplandy[1], **Marina Lévy**[2], **and Dennis J. McGillicuddy Jr.**[3]

[1]Geosciences Department, Princeton Environmental Institute, Princeton University, Princeton, NJ, USA, [2]Sorbonne Université, CNRS, IRD, MNHN, LOCEAN-IPSL, Paris, France, [3]Department of Applied Ocean Physics and Engineering, Woods Hole Oceanographic Institution, Woods Hole, MA, USA

Key Points:
- A high-resolution model simulates realistic hot spots of organic carbon export by physical subduction
- Eddy-driven subduction contributes little to annual export due to compensation between upward and downward fluxes
- Eddy-driven spatiotemporal variations in the mixed-layer efficiently export dissolved and particulate organic carbon

Supporting Information:
- Supporting Information S1

Correspondence to:
L. Resplandy,
laurer@princeton.edu

Citation:
Resplandy, L., Lévy, M., & McGillicuddy, D. J. Jr. (2019). Effects of eddy-driven subduction on ocean biological carbon pump. *Global Biogeochemical Cycles*, *33*. https://doi.org/10.1029/2018GB006125

Received 5 NOV 2018
Accepted 25 JUL 2019
Accepted article online 1 AUG 2019

©2019. American Geophysical Union. All Rights Reserved.

Abstract Estimates of the ocean biological carbon pump are limited by uncertainties in the magnitude of the physical injection of particulate and dissolved organic carbon to the ocean interior. A major challenge is to evaluate the contribution of these physical pumps at small spatial and temporal scales (<100 km and <1 month). Here, we use a submesoscale permitting biophysical model covering a large domain representative of a subpolar and a subtropical gyre to quantify the impact of small-scale physical carbon pumps.The model successfully simulates intense eddy-driven subduction hot spots with a magnitude comparable to what has been observed in nature (1,000–6,000 mg C·m^{-2}·day^{-1}). These eddy-driven subduction events are able to transfer carbon below the mixed-layer, down to 500- to 1,000-m depth. However, they contribute <5% to the annual flux at the scale of the basin, due to strong compensation between upward and downward fluxes. The model also simulates hot spots of export associated with small-scale heterogeneity of the mixed layer, which intermittently export large amounts of suspended particulate and dissolved organic carbon. The mixed-layer pump contributes ~20% to the annual flux. High-resolution measurements of export flux are needed to test models such as this one and to improve our mechanistic understanding of the biological pump and how it will respond to climate change.

1. Introduction

The oceanic biological carbon pump draws down atmospheric CO_2 by exporting particulate and dissolved organic carbon (POC and DOC) produced at the surface by marine ecosystems to the deep ocean (Falkowski et al., 1998). Estimates of the global carbon export associated with the biological pump vary widely between 5 and 15 Gt/year (Boyd & Trull, 2007; Boyd et al., 2019; DeVries & Weber, 2017; Dunne et al., 2007; Henson et al., 2011, 2012; Laws et al., 2000; Schlitzer, 2004; Siegel et al., 2014). Achieving a better constraint on the magnitude of the biological pump is difficult because it requires the characterization of multiple biological and physical processes that transfer and transform organic carbon. A particularly daunting challenge is to quantify the impact of processes occurring at small spatial and temporal scales (scales <100 km and <10 days) on the export flux at annual and large spatial scales ($\mathcal{O}$1,000 km).

At large spatial scale, the export is dominated by the passive sinking of POC produced in the well lit surface layer or euphotic zone—referred to as the *gravitational pump*. Two physical processes complement the gravitational pump: the deepening of the mixed layer that carries organic carbon out of the euphotic zone and leaves it behind during restratification—referred as the *mixed-layer pump*—and Ekman pumping of organic carbon associated with wind-driven ocean circulation—referred as the *Ekman pump*. Globally, the gravitational pump is estimated to be 4 to 9 Pg C/year (Bopp et al., 2013; Boyd et al., 2019; DeVries & Weber, 2017; Siegel et al., 2014) and the mixed-layer pump around 2.0–2.4 Pg C/year (corresponding to annual exports of 1.9 Pg of DOC and 0.1–0.5 Pg of POC, Hansell et al., 2009; Dall'Olmo et al., 2016). The Ekman pump is considered to be weaker and around 0.7 Pg C/year because of compensation between regions of downward and upward Ekman pumping (Lévy et al., 2013).

Fine-scale measurements have, however, revealed that POC export can be intensified at the center of ocean mesoscale eddies or in frontal structures at their periphery (Benitez-Nelson et al., 2007; Buesseler et al., 2009; Estapa et al., 2015; Guidi et al., 2012; McGillicuddy et al., 2007; Newton et al., 1994; Omand et al., 2015; Waite et al., 2016; Stukel, Aluwihare, et al. 2017; Stukel, Song, et al. 2017). Observations have also highlighted the presence of localized maxima in POC concentrations below the base of the euphotic layer,

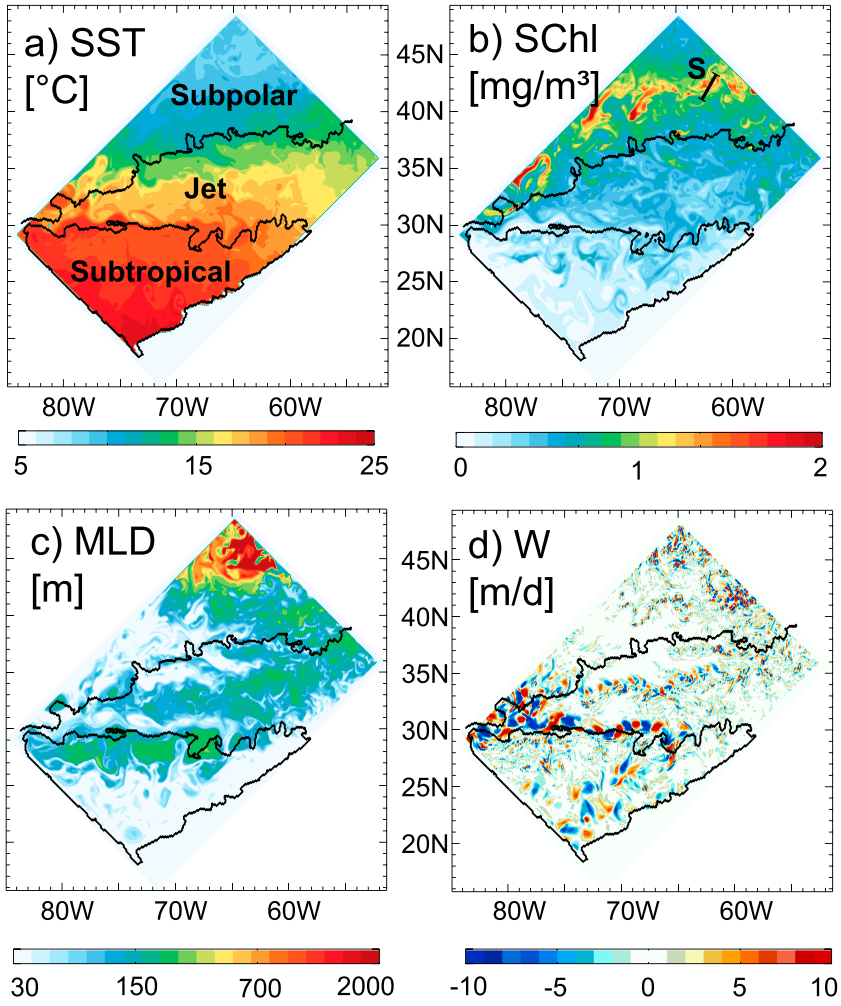

Figure 1. Spatial variability from basin scale to eddy scale over the model's idealized domain on 21 March: (a) sea surface temperature (SST), (b) surface chlorophyll (SChl), (c) mixed-layer depth (MLD), and (d) vertical velocity at 100-m depth (W). Upward vertical velocities are positive. Subtropical, jet, and subpolar regions are delimited by annual SChl concentrations thresholds of 0.15 and 0.3 mg/m^3 (black lines; Resplandy et al., 2012). Vertical Section S used in Figure 2 is shown in panel (b).

which are interpreted as evidence of small-scale physical subduction of POC (Llort et al., 2018; Omand et al., 2015; Stukel, Aluwihare, et al.2017). High-resolution biophysical models suggest that these subuduction "hot spots" are sustained by intense downward vertical velocities of the order of 1–100 m/day that can locally subduct POC (Karleskind et al., 2011; Lévy et al., 2001; Omand et al., 2015). These ageostrophic velocities ensue both from mesoscale dynamics and submesoscale frontal dynamics. Here we will use the generic term "eddy-driven" vertical velocity, to refer to the range of (sub)-mesoscale dynamics, that is, in the scale range 1–100 km. This *eddy pump* of POC could account for 20% to 70% of the local organic carbon export at the base of the euphotic layer (Llort et al., 2018; Omand et al., 2015; Stukel, Aluwihare, et al.2017, Stukel, Song, et al. 2017; Stukel & Ducklow, 2017) and has been identified as a potential pathway to transfer carbon to depths below the reach of the seasonal mixed layer (Erickson & Thompson, 2018). Nevertheless, previous observational and fine-scale model estimates of the eddy pump were limited in space and time (typically a few eddy structures over a few weeks/months and the upper 100 m) and excluded the eddy effects on the subduction of DOC. The integrated effect of the eddy pump on the biological carbon pump and its efficiency at exporting carbon to depth are therefore still poorly constrained.

The traditional view that the gravitational pump and mixed-layer pump operate solely on large scales is also being reassessed. Studies have shown that upward vertical velocities associated with eddies and fronts can supply nutrients to the euphotic zone, locally promote biological production, and eventually modulate the

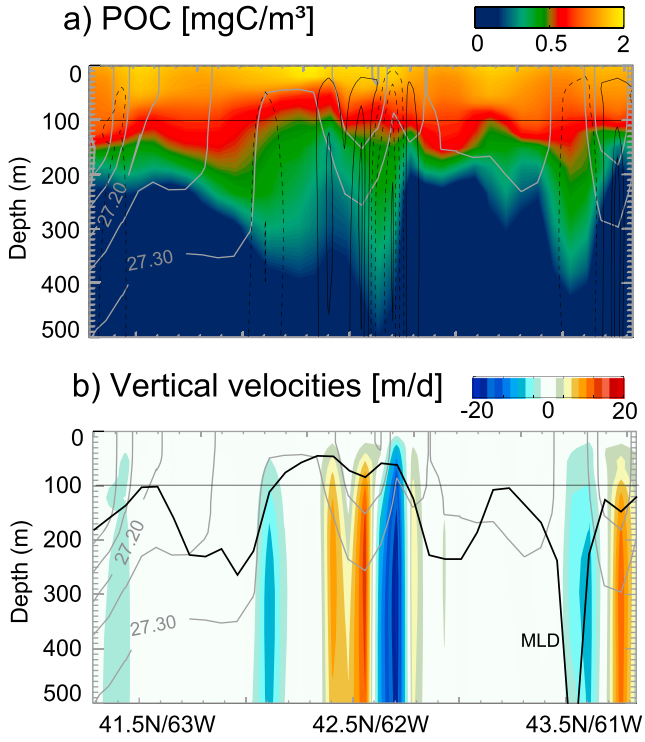

Figure 2. Eddy-driven export hot spots on 21 March along Section S (see position in Figure 1b). (a) Model particulate organic carbon (sinking + suspended POC) and vertical velocities (black contours, dashed downward, and solid upward). (b) Model vertical velocities and MLD (black). POC export hot spots across the base of the euphotic zone (100 m) are collocated with intensified vertical velocities at frontal regions. Negative velocities are downward. Density contours are indicated in gray. MLD = mixed-layer depth; POC = particulate organic carbon.

sinking of POC (e.g., Harrison et al., 2018; Lévy et al., 2012; Mahadevan, 2016; McGillicuddy, 2016). This dynamically driven variability in the gravitational pump could be further reenforced by biological processes, such as zooplankton diel and seasonal vertical migrations, which are expected to locally add 10% to 200% to the passive sinking flux of POC (Jónasdóttir et al., 2015; Steinberg & Landry, 2017). Eddies and fronts are also known to introduce spatiotemporal variations in the mixed-layer depth, as they can locally restratify or destratify the water column and modulate the large-scale seasonal patterns in mixed-layer depth (Dufois et al., 2014, 2016; Hausmann et al., 2017; Karleskind et al., 2011; Mahadevan, 2016). Yet the effect of eddies and fronts on the mixed-layer carbon pump has not been quantified (Dall'Olmo et al., 2016; Hansell et al., 2009; Lévy et al., 2013).

In this study we address some of these open questions. We characterize how the gravitational and physical subduction pumps vary in space and time, quantify how export hot spots occurring at small spatial scales (<100 km) influence the large-scale and seasonal patterns of the export flux, and examine how they might transfer carbon below the euphotic zone and the mixed layer. We use a high-resolution (2 km) biophysical model of a double gyre system that captures the mesoscale and part of the submesoscale dynamics (Lévy et al., 2010, 2012). The model, run over a repeating seasonal cycle, captures the intense frontal and mesoscale activity necessary to represent export hot spots as well as the regional contrasts between the warm low-chlorophyll waters of the subtropical gyre and the cold high-chlorophyll waters of the subpolar gyre (Figure 1, see validation and details in section 2). In the following, section 2 presents the model and how the gravitational, eddy, mixed-layer, and Ekman pumps are calculated. In section 3, we examine how the different pumps control the spatial and temporal variability of the organic carbon export flux and quantify their contribution to the annual export at the base of the euphotic zone and their efficiency at transferring carbon deeper in the water column. Finally, section 4 discusses the implications for measuring and estimating carbon export budgets.

2. Methods

2.1. Idealized North Atlantic Model—Description and Evaluation

This model is based on the free surface primitive equation ocean model NEMO (Madec, 2008), with 30 z coordinate vertical layers (10 to 20 m in the upper 100 m and 300 m at the bottom), forced with seasonal zonal profiles of wind, solar radiation, heat, and salt fluxes. We used the physical fields of Lévy et al. (2010) computed at a horizontal resolution of (1/54)° (2 km). The spectral analysis of the velocities in this simulation has revealed that the resolved scales are close to (1/9)° (i.e., ~10 km; Lévy et al., 2012). Moreover, Lévy, Resplandy, et al. (2012) have shown that the off-line advection of a tracer by the velocities computed on a (1/54)° grid at full resolution or degraded down to (1/9)° produces patterns that are almost indistinguishable (see their Figure 7). This methodology has the advantage to greatly reduce the numerical cost of the simulation while retaining the strength of the horizontal and vertical velocities produced by the original (1/54)° model (see details in Lévy, Resplandy, et al., 2012). Therefore, here we used these degraded fields to transport and compute the evolution of the biogeochemical tracers off-line.

The biogeochemical module used here is the LOBSTER version described in Resplandy, Lévy, et al. (2012), which includes phytoplankton, zooplankton, semilabile dissolved organic material (DOM, 5-month time scale), nitrate, ammonium, and two classes of sinking detritus (slow and fast sinking rates of 5 and 200 m/day). Aggregation and disaggregation of detritus and DOM take into account differential settling and turbulence coagulation mechanisms (Resplandy et al., 2012). We use a constant carbon to nitrogen C:N ratio of 6.6 (Redfield proportions) for both POC and DOC. Detailed description and evaluation of the physical and biological dynamics of the model can be found in Lévy et al. (2010), Lévy, Iovino, et al. (2012), and

Resplandy, Martin, et al. (2012). The spatiotemporal evolution of surface chlorophyll, mixed-layer depth, and surface POC and DOC is shown in supporting information Video S1.

The GYRE model reproduces the large-scale distribution of temperature, surface chlorophyll, and the particulate export expected from thorium deficit measurements in the North Atlantic (see details in Resplandy et al., 2012). It also simulates the features of export hot spots observed in nature. Figure 2 shows three vertical intrusions of POC associated with intensified downward vertical velocities along eddy-driven fronts. These intrusions extend down to 400 m in the model, similar to what has been measured in the North Atlantic (Omand et al., 2015). Finally, the model reproduces subsurface maxima in POC concentrations between the base of the euphotic layer and 600 m (Figure S1), which have been observed in situ and previously used to quantify the strength of the eddy subduction pump (Llort et al., 2018; Omand et al., 2015; Stukel, Aluwihare, et al. 2017).

Daily maps of the spatial variability in model physical (sea surface temperature, mixed-layer depth, and vertical velocity) and biological (chlorophyll, POC, and DOC concentrations) fields are shown in Figures 1 and S2 and Video S1.

2.2. Pumps of Organic Carbon

For each tracer C (C can be fast sinking POC, slow sinking POC, and suspended POC or DOC), the total export E_C is computed off-line as the sum of the gravitational and subduction pumps:

$$E_C = E_{\text{gravitational}} + E_{\text{subduction}}. \tag{1}$$

We further decompose the *subduction pump* into three contributions: the advective flux associated with large-scale Ekman pumping (Ekman pump), the eddy-driven advective flux arising from spatiotemporal variations in vertical velocities and organic carbon (eddy pump), and the export associated with vertical mixing (mixed-layer pump):

$$E_{\text{subduction}} = E_{\text{Ekman}} + E_{\text{eddy}} + E_{\text{mixed layer}}. \tag{2}$$

All terms are computed as a function of depth. Note that in the literature, subduction sometimes includes the mixed-layer pump and the eddy pump (Stukel, Song, et al. 2017), the mixed-layer pump and the Ekman pump (Lévy et al., 2013), or only the eddy pump (Omand et al., 2015).

The gravitational pump across the depth level z is computed from the sinking speed V_C of tracer C ($V_C > 0$ for slow and fast sinking POC and $V_C = 0$ for suspended POC and DOC) and the concentration in tracer C at depth z and time step t ($C(t,z)$):

$$E_{\text{gravitational}} = - \quad V_C \times \quad C(t,z). \tag{3}$$

The Ekman pump at depth z is computed from the annual mean concentration at depth z ($\overline{C(z)}$ and annual mean vertical velocity at depth $z\overline{w(z)}$ (overbar indicates the annual average):

$$E_{\text{Ekman}} = - \quad \overline{w(z)} \times \overline{C(z)}. \tag{4}$$

The eddy pump is the residual between the total model vertical advective flux at depth z and time t and the annual Ekman pump at the same depth. It includes spatiotemporal covariations between vertical velocity $w(t,z)$ and concentrations $C(t,z)$:

$$E_{\text{eddy}} = - \quad w(t,z)' \times C(t,z)' \tag{5}$$

$$\text{with} \quad w(t,z)' = \quad w(t,z) - \overline{w(z)} \quad \text{and} \quad C(t,z)' = C(t,z) - \overline{C(z)}.$$

The mixed-layer pump is often evaluated as a detrainment term assuming an homogeneous concentration of tracer in the mixed layer (e.g., Dall'Olmo et al., 2016). Here, however, we use the spatiotemporally varying POC and DOC profiles and simulated vertical diffusivities. Note that using the entrainment method would introduce differences of the order of 5–10% in the mixed-layer pump due to the assumption of homogeneity in the mixed layer. The mixed-layer pump at time t and depth z is computed using the model vertical diffusion coefficient K_z ($\text{m}^{-2}\cdot\text{s}^{-1}$) and the vertical gradient in tracer C:

$$E_{\text{mixed layer}} = K_z(t,z) \quad \times \frac{\partial C(t,z)}{\partial z} \tag{6}$$

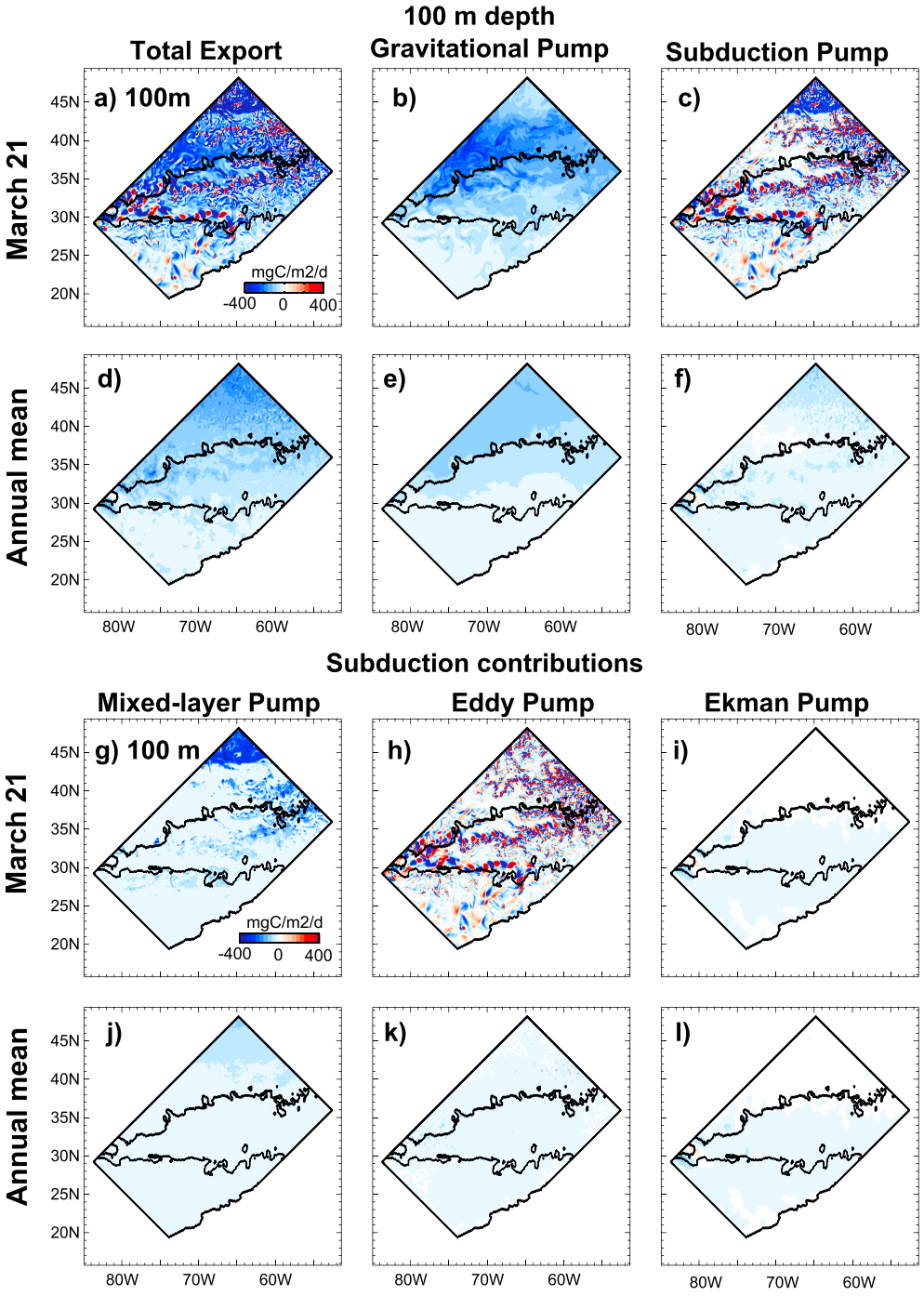

Figure 3. Export of organic carbon out of the euphotic zone (100 m) in the GYRE model. The total export of dissolved organic carbon and particulate organic carbon composed of the contributions from the gravitational and subduction pumps. The subduction pump is further decomposed into the mixed-layer, eddy, and Ekman pumps. Export contributions are shown on 21 March during the spring bloom (a–c and g–i) and averaged annually (d–f and j–l). Negative values indicate a downward export and positive values an upward transport.

These calculations are done from 2-day model average results using a 360-day annual calendar. The seasonal cycle of POC, DOC, and the contribution from the different pumps in the subtropical, subpolar, and jet regions is shown in Figures S3 and S4. The spatiotemporal evolution of the pumps and the total export of organic carbon are shown in supporting information Video S2.

For each pump, we compute the probability density distribution of the local export, that is, at each model point, and the probability density distribution of the export averaged in 100 by 100-km boxes (Figure 4). There are 40,824 points and 551 one hundred kilometer boxes per time step in the model domain and 180 time steps (2-day averaged fields), yielding 7,348,320 local export estimates (Figures 4a and 4b) and 99,180 estimates averaged on scales of 100 km (Figures 4c and 4d). Monthly maps of the gravitational pump and subduction pump averaged in 100 by 100-km boxes and the spatiotemporal variability of these pumps in these boxes are shown in the supporting information.

3. Results

3.1. Carbon Pumps Spatial Variability at the Base of Euphotic Layer

A starting point for quantifying spatial variability is to consider the daily export flux of total organic carbon (POC + DOC) simulated at the peak of the spring bloom (here we use 21 March). As shown in Figure 3, the total export flux on 21 March shows a basin-scale south-to-north gradient strongly modulated by export hot spots (defined here with an arbitrary threshold of local export >400 mg C·m^{-2}·day^{-1}). Locally, the export flux on that day can exceed 1,000 mg C·m^{-2}·day^{-1} (up to 4,000 mg C·m^{-2}·day^{-1}) and shows variations up to 800 mg C·m^{-2}·day^{-1} on scales smaller than 100 km.

The background south-to-north gradient in export is largely imposed by the gravitational pump. On March 21, phytoplankton are blooming in the subpolar gyre around 40°N (Figure 1), and the gravitational export is highest on the southern flank of the actively blooming region (30°N to 40°N) due to the 1- to 2-week lag between the peak in surface phytoplankton and the peak in particle export (Figure 3b). As previously shown in Resplandy et al. (2012), the simulated south-to-north gradient in the gravitational pump falls within the range of values expected from thorium deficit measured during spring and summer in the subtropical, jet, and subpolar North Atlantic regions. At smaller scales, hot spots in the gravitational pump are localized in filaments wrapped around eddy structures (Figure 3b) and mirror the spring bloom patterns delineated by surface Chl and POC concentrations (Figures 1b and S2). The variability of the gravitational pump in the model is in agreement with high-resolution measurements in the subtropical gyre and jet region that shows variations in the sinking flux on the order of 5–30 mg C·m^{-2} · day^{-1} over 40-km transects (see Figure 8 and 10 in Estapa et al., 2015).

Locally, most intense export fluxes are controlled by the subduction pump and in particular the eddy pump (Figures 3c and 3h). The eddy pump follows the patchiness of the vertical velocity field, with hot spots localized at fronts where vertical velocities are larger than 50 m/day (Figure 1d). These hot spots can locally reenforce (negative values), balance, or even reverse (positive values) the export of sinking particles by bringing organic carbon back into the euphotic zone (Figure 3h). The mixed-layer pump is also patchy (Figure 3g). On 21 March, this pump mostly exports organic carbon in the northern subpolar gyre but modulations of the mixed layer at spatial scales smaller than 100 km in the jet region (Figure 1c) locally suppress or enhance the export in specific frontal and mesoscale features.

Figure 4 generalizes the results obtained for 21 March and quantifies how each pump contributes to export hot spots at scales <100 km over the model domain and full seasonal cycle. As suggested by the daily export field, the dynamical spatial variability influences the subduction pump more than the gravitational pump. The eddy pump can locally subduct up to 6,000 mg C·m^{-2}·day^{-1} and upwell up to 4,000 mg C·m^{-2}·day^{-1}, the mixed-layer pump can subduct up to 1,500 mg C·m^{-2}·day^{-1}, while hot spots in the gravitational pump never exceed 1,000 mg C·m^{-2}·day^{-1} (Figures 4a and 4b). Yet we find that gravitational hot spots are more efficient at exporting organic carbon than subduction hot spots. We evaluate the impact of hot spots on the export at larger scale by comparing the local export (at each model point) with the export averaged over spatial scale of 100 km. The gravitational pump shows no damping of the export flux when averaged over 100 km (similar probability density distribution in Figures 4a and 4c). In contrast, subduction hot spots occurring at scales <100 km largely balance when averaged over 100-km areas (tapering of extremes in probability density distribution by a factor of 10 from −6,000 to −600 mg C·m^{-2}·day^{-1}, Figures 4a and 4c).

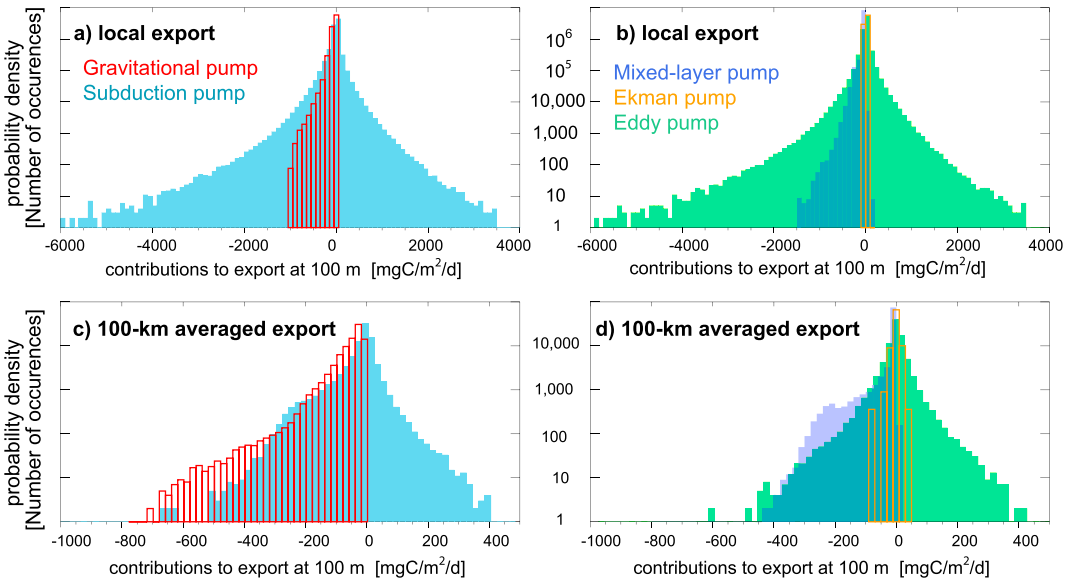

Figure 4. Export at 100-m depth. (a and b) Local export at each model point and (c and d) averaged over 100 km × 100 km. Gravitational and subduction pumps (a, c) and contributions to subduction from mixed-layer, eddy, and Ekman pumps (b, d). Distribution densities are the number of model points (a and b) or 100-km × 100-km model boxes (c and d) with a certain value of export. The total number of model points is 7,348,320, and the total number of 100-km × 100-km model boxes is 99,180 (see section 2). Monthly maps of the mean export and its spatiotemporal variability in the 100-km × 100-km boxes are shown in the supporting information.

In the model, the weak contribution of the eddy pump at spatial scales of 100 km is explained by a strong compensation between downward and upward vertical transport. Although downward hot spots can be larger than upward hot spots (probability density distribution is not symmetric in Figure 4b), the eddy pump falls below 500 mg C·m^{-2}·day^{-1} when averaged over spatial scales of 100 km (Figure 4d). The mixed-layer pump is predominantly exporting carbon downward (negative values, Figure 4b), but as shown in the daily export flux this pump is patchy and the effect of mixed-layer export hot spots is dampened by contiguous areas of no export (Figure 3d). As a result, the mixed-layer pump also falls below 500 mg C·m^{-2}·day^{-1} when averaged over spatial scales of 100 km (Figure 4d).

3.2. Subduction Hot Spots Modulate Export Seasonal Cycle

As shown by three cases studies in Figure 5, the export flux and the contributions from the different pumps also vary in time. On seasonal time scales, the export is dominated by the gravitational pump and the mixed-layer pump (solid lines indicate average in 100 × 100-km areas). The export in the northern subpolar gyre (Box 1) follows the canonical succession of export by the mixed-layer pump in winter and early spring (200–300 mg C·m^{-2}·day^{-1}), sinking of particles produced during the spring bloom (600 mg C·m^{-2}·day^{-1}), followed by a weaker export flux during summer and fall (100 mg C·m^{-2}·day^{-1}, Figures 5a and 5b). The magnitude of this seasonal cycle gradually decreases southward into the jet region (mixed-layer and gravitational pumps <200 mg C·m^{-2}·day^{-1} in Box 2, Figures 5c and 5d) and disappear in the subtropical gyre (mixed-layer and gravitational pumps <10 mg C·m^{-2}·day^{-1} in Box 3, Figures 5e and 5f).

On shorter time scales (days to months), the export flux is strongly influenced by the dynamical variability and subduction at small spatial scales. We quantify the impact of spatial variability on the seasonal cycle using the variability of the export flux within the 100-km case study area (shading in Figure 5 is the ±1 spatial standard deviation in 100 × 100-km areas). The eddy pump can locally introduce short-term variations of at least 25–50 mg C·m^{-2}·day^{-1} yearround in the three areas, and variations as high as 1,000 mg C·m^{-2}·day^{-1} due to specific frontal and eddy features such as the sharp front that passes through Box 1 in August/September (Figures 5b and S5). The gravitational and mixed-layer pumps can introduce short-lived variations of 100–400 mg C·m^{-2}·day^{-1} in the export flux, but this process is limited in space and time to the subpolar gyre and jet regions during winter and spring (Figures 5b and 5d). The patchiness of these two pumps is otherwise weaker and <50 mg C·m^{-2}·day^{-1}.

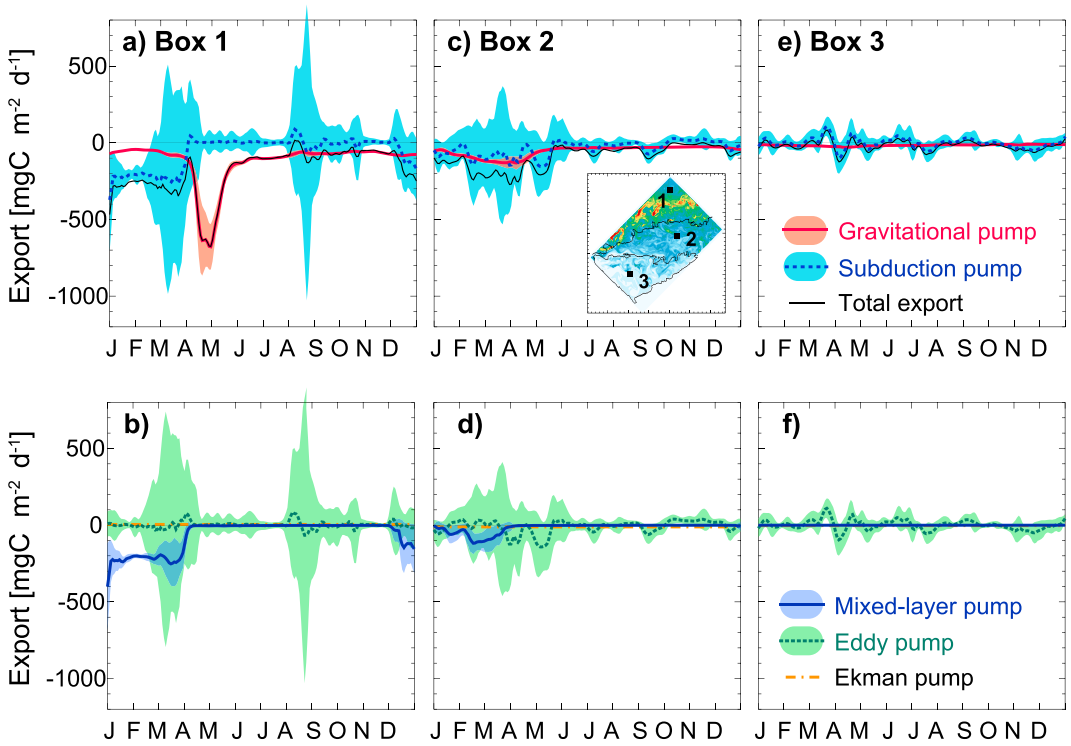

Figure 5. Seasonal and regional variations in export flux at the base of the euphotic zone (100-m depth). The gravitational and subduction pumps (a, b) and individual contributions to the subduction pump (mixed-layer, eddy, and Ekman pumps, [e, f]) are compared in three 100-km × 100-km case studies ([a, b] Box 1 in subpolar gyre, [c, d] Box 2 in jet region, and [e, f] Box 3 in subtropical gyre). The mean (solid lines) and the export variability on spatial scales smaller than 100 km (shading indicates ±1 spatial standard deviation) are shown for each box. The seasonal evolution of dissolved organic carbon and particulate organic carbon in Boxes 1 to 3 is shown in Figure S3, and the export pumps averaged over the subtropical gyre, jet region, and subpolar gyre are shown in Figure S4.

3.3. Eddy Pump Contributes Little to Annual and Regional Budgets

On annual average, the export of organic carbon at the base of the euphotic zone is 30 mg C·m^{-2}·day^{-1} in the subtropical gyre, 70 mg C·m^{-2}·day^{-1} in the jet region, and 120 mg C·m^{-2}·day^{-1} in the northern subpolar gyre (Figure 3d, spatial mean over each regions). The gravitational pump accounts for 73% of this annual carbon export over the domain, while the subduction pump in comparison only accounts for the remaining 27% (Figures 3e, 3f, and 8). The mixed-layer pump alone accounts for 22% of the annual organic carbon export over the domain (i.e., 80% of the subduction pump) but is mostly confined to the subpolar gyre. Despite the presence of strong hot spots, the eddy pump accounts for 4% of the annual export at 100 m at the basin scale, which is similar in magnitude to the contribution of large-scale Ekman pumping found in this study (1%) and derived from global ocean simulations (7% in Lévy et al., 2013).

Although the eddy pump and Ekman pump (i.e., advective subduction pumps) contribute little to the annual export over the domain, our results suggest that together these two pumps export more than 60% of the DOC in the jet and subtropical gyre where the mixed-layer pump is weak (Figure 8). This result is consistent with a recent study suggesting that the export of DOC is a major contributor to the export of organic carbon in subtropical gyres (Roshan & DeVries, 2017). Their diagnostic approach does not resolve eddy-driven dynamics and the biological processes producing and decomposing DOC explicitly, but it demonstrates the need for a large export of DOC to reconcile surface DOC production with observed ocean tracer distributions. Our results suggest that subduction could sustain the DOC pump in subtropical gyres inferred by Roshan and DeVries (2017). Finally, we also note that in the subpolar gyre, the Ekman pump yields a weak reemergence of DOC (upward transport of 5.0 mg C·m^{-2}·day^{-1} into the euphotic zone) because of the large DOC export by the mixed-layer pump in winter, which becomes available for upward vertical transport after spring restratification.

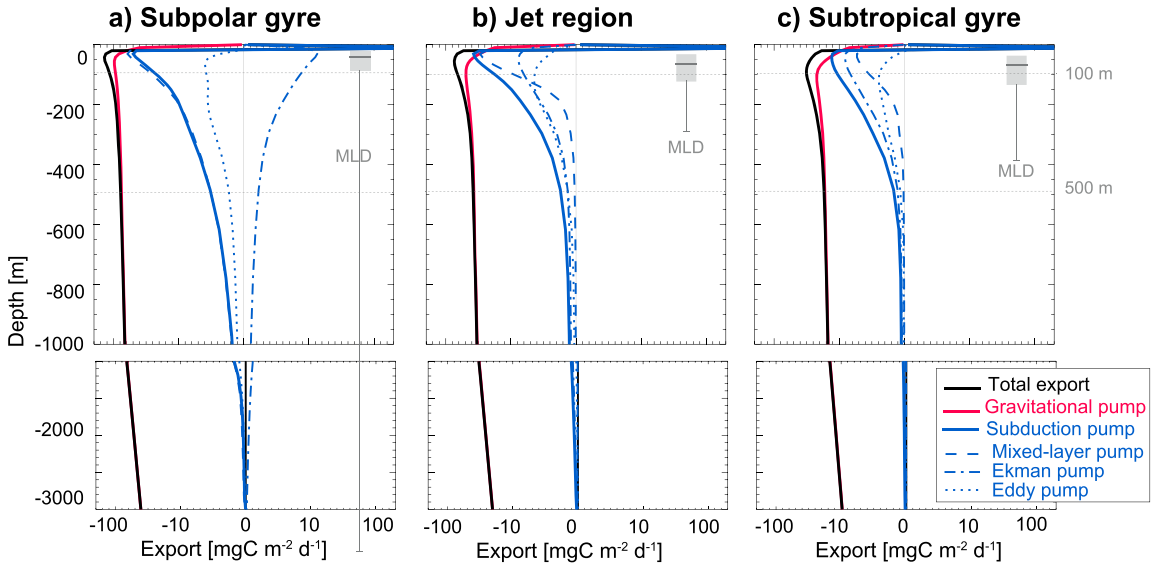

Figure 6. Depth profiles of annual mean export of organic carbon in the subpolar, jet, and subtropical regions. Total export sums the gravitational and subduction pumps. The subduction pump is decomposed into contributions from mixed-layer, eddy, and Ekman pumps. Box plots of the maximum winter mixed-layer depth (MLD) are shown (median, first and third quartiles, and minimum and maximum values in each region). Export is in log scale.

3.4. Can the Eddy Pump Transfer Carbon Deeper in Water Column?

In the model, the contribution of the subduction pump declines with depth, and at 500 m it only accounts for 2% of the annual organic carbon export, the gravitational pump accounting for the remaining 98% (Table S1 and Figure S6). Yet, in regions of deep convective winter mixed layer (such as the northern subpolar gyre in our model), the mixed-layer pump can subduct carbon as deep as 500–1,000 m (Figures 6 and S6). In regions of shallower winter mixed layer (jet and subtropical gyre), the mixed-layer pump is limited to the upper 100–200 m but the eddy pump acts as a relay, transferring carbon below the mixed layer (eddy pump maximum right below the mixed-layer pump maximum in Figures 6b and 6c).

The individual depth profiles of the eddy pump shown in Figure 7 suggest its effect is generally confined to the mixed-layer but can, in some cases, export as much as 500 mg C·m^{-2}·day^{-1} below the depth of the mixed layer (e.g., Profiles 1 to 5). However, because these events are relatively rare and limited in space and time, their contribution to the annual and regional carbon export is still about 10 times smaller than the gravitational pump (Figure 6). This result is consistent with the study of Stukel, Song, et al. (2017), which showed that, in the California Current, sinking particles were more efficiently exported at depth than subducted particles.

4. Discussion

4.1. Implications and Link to In Situ Measurements

We find that the export of total organic carbon simulated in an idealized double gyre system is highly variable at the eddy scale (that is 100 km and below). Locally, largest export fluxes are sustained by the eddy-driven subduction pump. Simulated hot spots of export up to 1,000–6,000 mg C·m^{-2}·day^{-1} are consistent with previous observations and modeling work focusing on the export along a frontal structure during the subpolar North Atlantic Spring bloom (Omand et al., 2015, see their Figure S12). However, we find that these eddy-driven hot spots contribute less than 5% to the export of organic carbon on annual and regional average. Our model suggests that although hot spots associated with particle sinking (up to 1,000 mg C·m^{-2}·day^{-1}) and vertical mixed layer (up to 1,500 mg C·m^{-2}·day^{-1}) are weaker than those of the eddy pump, they are more efficient at exporting carbon.

On annual average and over the domain, the gravitational pump exports 73% and the mixed-layer pump 22% of the total organic carbon. This result appears consistent with the traditional view of the biological pump—dominated by gravitational pump—and mixed-layer pump. A major difference, however, is that in the traditional view, the influence of the mixed-layer pump at the global scale is attributed to the wintertime

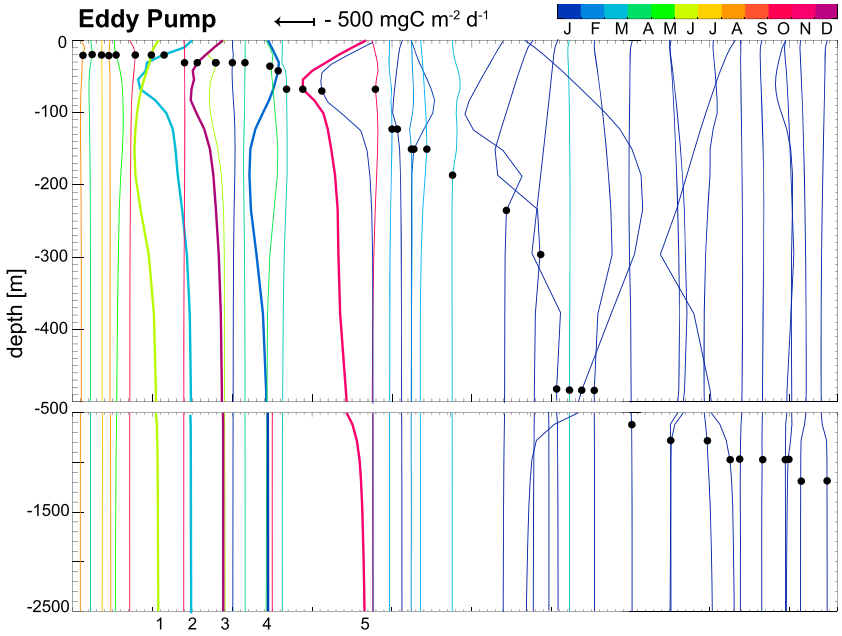

Figure 7. Eddy pump export (downward transport <0 or upward transport >0) along randomly picked depth profiles in the model. Mixed-layer depth (black dots) and month of year (colors) are indicated for each profile. Profiles 1 to 5 (thick lines) show eddy pump exporting below the mixed layer.

export of DOC accumulated over the spring and summer seasons (Hansell et al., 2009; Henson et al., 2012), while in our model the mixed-layer pump exports DOC but also large amounts of suspended POC (plankton) at 100 m (Figure 8b and Table S1). This downward mixing of suspended POC is associated with eddy-driven subseasonal variations in the mixed-layer depth. Short-lived restratification events (time scale of days) promote not only plankton growth (Mahadevan et al., 2011) but also the export of recently produced suspended POC during the subsequent deepening of the mixed layer. This efficient mixing of suspended POC accounts for half of the simulated annual subduction pump and about 10–15% of the total export at 100-m depth. This result is supported by recent glider optical observations suggesting that high-frequency vertical mixing of small POC could account for 5–25% of the annual export in the North Atlantic Porcupine Abyssal Plain (49°N to 16°W; Bol et al., 2018). The global export of POC by restratification/destratification was estimated to be 0.1–0.5 Pg C/year using satellite-based POC and float-based mixed-layer depths (Dall'Olmo et al., 2016). Our modeling results suggest that heterogeneities in the mixed layer at small spatial scale play a critical role in sustaining this export of suspended POC.

In our model, eddy pump hot spots are associated with downward eddy-driven vertical velocities larger than 50 m/day, localized at fronts. These vigorous downward motions are short-lived and compensated by upward velocities. This compensation between upward and downward eddy-driven transport occurs in part at spatial scales of ~100 km and in part at larger spatial and temporal scales. The compensation between upward and downward transport is, however, not complete. In line with previous observations and modeling studies (Llort et al., 2018; Omand et al., 2015; Stukel, Aluwihare, et al.2017; Stukel, Song, et al.2017), we find that the downward transport of POC across the euphotic layer (8 mg $C{\cdot}m^{-2}{\cdot}day^{-1}$) exceeds the upward transport of POC (7 mg $C{\cdot}m^{-2}{\cdot}day^{-1}$) because of the asymmetric effect of upward and downward velocities on the vertical gradient in particles (sharp decline with depth, Figure 2). The integrated effect of eddy-driven POC subduction is, however, small and accounts for less than 2% of the annual POC export at the regional scale.

This contrasts with the results of a recent study that found very little compensation between upward and downward transports because of a high correlation between high POC concentrations and downward vertical velocities in their model (Omand et al., 2015). In our case, the correlation between high POC values and downward velocities is weak (Pearson correlation coefficient $R = -0.14$ for 150-m POC concentrations >15 mg C/m^3). A major difference is the more complex biological model used in our study, including nutrients, DOC, phytoplankton, zooplankton, and detritus, as well as a representation of the

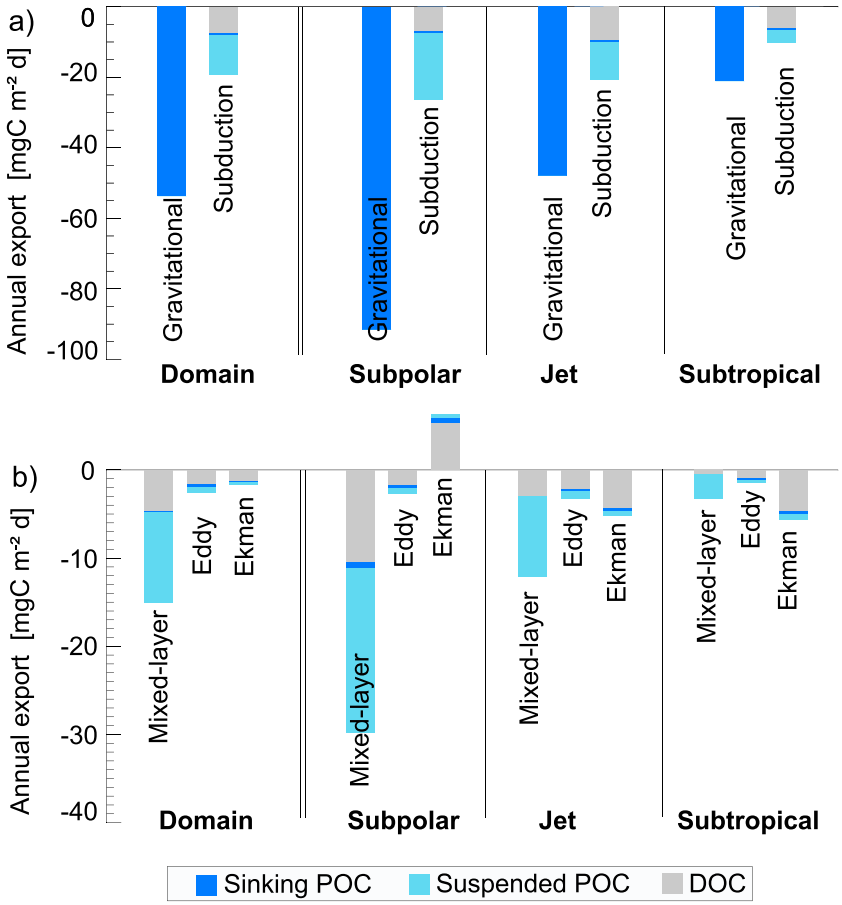

Figure 8. Annual export of dissolved organic carbon (DOC) and particulate organic carbon (POC; sinking and suspended) at 100 m averaged over the model domain and over the subpolar, jet, and subtropical regions. (a) Export from the gravitational and subduction pumps and (b) contributions to the subduction pump from the mixed-layer, eddy, and Ekman pumps. Export fluxes are downward (negative) except for the Ekman pump in the subpolar gyre. Export fluxes are given in Table S1.

aggregation/fragmentation effect of turbulence and the funneling effect of eddies on detritus (Alldredge et al., 2003; Waite et al., 2016; see details in the supporting information). The resulting nonlinearities temporally decouple production, decay, and export of POC within the evolving 3-D velocity field. In nature, biological processes are more complex than what is represented in any of the models, and whether or not this additional complexity yields more or less coupling between downward velocities and plankton biomass remains to be assessed. A second factor in this comparison, however, is the lower horizontal resolution of our physical model (2 km vs. 1 km in Omand et al., 2015), which could yield weaker vertical velocities and underestimate the asymmetry between small-scale upwelling and downwelling across frontal structures (Gula et al., 2014; Mahadevan, 2016).

The magnitude of this compensation between eddy-driven upward and downward carbon transport is difficult to detect and quantify from in situ observations. Llort et al. (2018) developed an observation-based method to quantify the eddy-driven subduction of POC in the Southern Ocean, using subsurface maxima in POC detected by biogeochemical floats. By applying the same method to the POC in our model (see Text S1), we find an annual mean POC subduction of 0.6 mg $C{\cdot}m^{-2}{\cdot}day^{-1}$, which represents only a small fraction of the POC downward eddy pump (8 mg $C{\cdot}m^{-2}{\cdot}day^{-1}$) and about two thirds of the net POC export by the eddy pump (i.e., the sum of downward and upward transport that equals 1 mg$\cdot C{\cdot}m^{-2}{\cdot}day^{-1}$, Figure 8). The method successfully detected the strong downward subduction events simulated in the jet and subpolar regions, but by design it did not capture the weaker downward export events without POC subsurface signatures nor the upward obduction events (Figure S7). This comparison is, however, limited by the fact that the model vertical resolution at the subsurface (50–100 m) is lower than the float profile resolution (10–50 m),

so the model may underestimate the magnitude of subsurface POC signatures and associated subduction flux. In any case, we note that available observation-based methods to quantify eddy-driven subduction do not detect POC obduction events and therefore cannot be used to address the compensation of downward and upward POC flux events that we see in our model.

4.2. Caveats and Limitations

We acknowledge that there are some caveats in our approach, including the idealized representation of the double gyre system and the biogeochemical and ecosystem dynamics. Observational and modeling studies suggest that the active export of organic carbon by zooplankton vertical migration could add 30% to 50% to the gravitational pump in the North Atlantic (Hansen & Visser, 2016; Jónasdóttir et al., 2015; Steinberg & Landry, 2017) and likely contributes, along with the subduction pump examined here, to the spatial variability in the global biological pump. Zooplankton may also fragment part of the fast sinking large POC into slow sinking small POC and DOC that become more available to microbial respiration (Baker et al., 2017; Giering et al., 2014). Our model includes one class of zooplankton and some parameterization of the fragmentation and aggregation processes of POC linked to the flow turbulence and to zooplankton grazing (Resplandy et al., 2012) but does not represent the observed complexity in plankton/microbe dynamics.

Additional factors are the complex spectrum of lability and carbon to nitrogen (C:N) ratios observed in dissolved and particulate organic matter (Amon & Benner, 1994; Hansell, 2013; Hansell et al., 2015). Our model includes a semilabile DOM pool (remineralization time scale of 5 months), which is the pool controlling the seasonal accumulation and carbon export in the ocean (Hansell et al., 2015, Chapter 15.). However, our model probably underestimates the size of this pool in the subtropical gyre (observed concentrations of 10 μmol C·K·g^{-1} [Hansell, 2013] vs. simulated concentrations <4 μmol C·K·g^{-1}). The model does not include refractory and semirefractory pools of DOM. Given the temporal and spatial scales considered in this study (≤1 year, <3,000 km), refractory DOC has little influence on our results and would correspond to a constant background value equal to deep observed DOC concentrations (40 μmol·K·g^{-1}; Hansell et al., 2009). However, semirefractory DOC (remineralization time scale of years), which accumulates in subtropical gyres (10 μmol·K·g^{-1}), could enhance export in this region (Hansell, 2013). Finally, our approach ignores spatiotemporal variations in DOM lability and departures in the C:N stoichiometry that could yield a C-enriched DOM and an increased contribution of DOC to the total carbon export. For example, a C:N DOM ratio of 10 would increase the annual DOC export in the subtropical gyre by 50% and the annual carbon export in this region by 10%. Because of the limitations (DOM concentrations, lability, and C:N ratio), the relative contribution of DOM to the total export in the subtropical gyre could be larger than simulated in the model. Similarly, our approach does not represent variations in POC lability, which could increase the concentration of small particles and modify the carbon export out of the euphotic zone (Aumont et al., 2017; Baker et al., 2017). These biological processes are known to control the DOC and POC export fields on seasonal to interannual time scales and on regional to basin spatial scales. Nevertheless, their influence on the export at scales <100 km is still to be determined.

The idealized double gyre physical model used in this study resolves mesoscale eddies but does not fully resolve submesoscale dynamics, which would require a much higher horizontal resolution (McWilliams, 2016). It is therefore likely that the model underestimates vertical velocities and asymmetries in upward and downward transport (Gula et al., 2014; Mahadevan, 2016) and the strength of submesoscale instabilities (Erickson & Thompson, 2018). In addition, the model does not include high-frequency winds and could therefore underestimate the downward mixing and export of DOC and POC along frontal structures (Whitt et al., 2017). Another related caveat is the off-line computation used in our model, which filters the impact of internal waves. Recognizing these limitations, we expect the present study to give a lower bound of the export patchiness that can be expected in nature. High-resolution measurements of organic matter dynamics will be key to further constrain the impact of eddy-driven biological-physical interactions on the export flux, test and improve their representation in global and regional models such as the one used here, and refine estimates of the global biological carbon pump.

Acknowledgments
L. R. is funded by NASA EXPORTS Awards 80NSSC17K0555 and NNX16AR50G. D. J. M. gratefully acknowledges support of NSF and NASA Grant NNX16AR50G. M. L. is supported by Centre National d'Etudes Spatiales (CNES) and by the French Agence Nationale de la Recherche Award SOBUMPS ANR-16-CE01-0014. The model data are publicly available on Zenodo (zenodo.org/record/3064658#.XOWKMpNKhBw) under the DOI:10.5281/zenodo.3064658 website.

References

Alldredge, A. L., Granata, T. C., Gotschalk, C. C., & Dickey, T. D. (2003). The physical strength of marine snow and its implications for particle disaggregation in the ocean. *Limnology and Oceanography*, *35*(7), 1415–1428. https://doi.org/10.4319/lo.1990.35.7.1415

Amon, R. M. W., & Benner, R. (1994). Rapid cycling of high-molecular-weight dissolved organic matter in the ocean. *Nature*, *369*(6481), 549. https://doi.org/10.1038/369549a0

Aumont, O., van Hulten, M., Roy-Barman, M., Dutay, J.-C., Éthé, C., & Gehlen, M. (2017). Variable reactivity of particulate organic matter in a global ocean biogeochemical model. *Biogeosciences*, *14*(9), 2321–2341. https://doi.org/10.5194/bg-14-2321-2017

Baker, C. A., Henson, S. A., Cavan, E. L., Giering, S. L. C., Yool, A., Gehlen, M., et al. (2017). Slow-sinking particulate organic carbon in the Atlantic Ocean: Magnitude, flux, and potential controls: Slow-Sinking Particulate Organic Carbon. *Global Biogeochemical Cycles*, *31*, 1051–1065. https://doi.org/10.1002/2017GB005638

Benitez-Nelson, C. R., Bidigare, R. R., Dickey, T. D., Landry, M. R., Leonard, C. L., Brown, S. L., et al. (2007). Mesoscale eddies drive increased silica export in the subtropical Pacific Ocean. *Science*, *316*(5827), 1017–1021. https://doi.org/10.1126/science.1136221

Bol, R., Henson, S. A., Rumyantseva, A., & Briggs, N. (2018). High-frequency variability of small-particle carbon export flux in the Northeast Atlantic. *Global Biogeochemical Cycles*, *32*, 1803–1814. https://doi.org/10.1029/2018GB005963

Bopp, L., Resplandy, L., Orr, J. C., Doney, S. C., Dunne, J. P., Gehlen, M., et al. (2013). Multiple stressors of ocean ecosystems in the 21st century: Projections with CMIP5 models. *Biogeosciences*, *10*(10), 6225–6245. https://doi.org/10.5194/bg-10-6225-2013

Boyd, P. W., Claustre, H., Levy, M., Siegel, D. A., & Weber, T. (2019). Multi-faceted particle pumps drive carbon sequestration in the ocean. *Nature*, *568*(7752), 327–335. https://doi.org/10.1038/s41586-019-1098-2

Boyd, P. W., & Trull, T. W. (2007). Understanding the export of biogenic particles in oceanic waters: Is there consensus? *Progress in Oceanography*, *72*(4), 276–312. https://doi.org/10.1016/j.pocean.2006.10.007

Buesseler, K. O., Pike, S., Maiti, K., Lamborg, C. H., Siegel, D. A., & Trull, T. W. (2009). Thorium-234 as a tracer of spatial, temporal and vertical variability in particle flux in the North Pacific. *Deep Sea Research Part I: Oceanographic Research Papers*, *56*(7), 1143–1167. https://doi.org/10.1016/j.dsr.2009.04.001

Dall'Olmo, G., Dingle, J., Polimene, L., Brewin, R. J. W., & Claustre, H. (2016). Substantial energy input to the mesopelagic ecosystem from the seasonal mixed-layer pump. *Nature Geoscience*, *9*(11), 820–823. https://doi.org/10.1038/ngeo2818

DeVries, T., & Weber, T. (2017). The export and fate of organic matter in the ocean: New constraints from combining satellite and oceanographic tracer observations. *Global Biogeochemical Cycles*, *31*, 535–555. https://doi.org/10.1002/2016GB005551

Dufois, F., Hardman-Mountford, N. J., Greenwood, J., Richardson, A. J., Feng, M., Herbette, S., & Matear, R. (2014). Impact of eddies on surface chlorophyll in the South Indian Ocean. *Journal of Geophysical Research: Oceans*, *119*, 8061–8077. https://doi.org/10.1002/2014JC010164

Dufois, F., Hardman-Mountford, N. J., Greenwood, J., Richardson, A. J., Feng, M., & Matear, R. J. (2016). Anticyclonic eddies are more productive than cyclonic eddies in subtropical gyres because of winter mixing. *Science Advances*, *2*(5), e1600282. https://doi.org/10.1126/sciadv.1600282

Dunne, J. P., Sarmiento, J. L., & Gnanadesikan, A. (2007). A synthesis of global particle export from the surface ocean and cycling through the ocean interior and on the seafloor. *Global Biogeochemical Cycles*, *21*, GB4006. https://doi.org/10.1029/2006GB002907

Erickson, Z. K., & Thompson, A. F. (2018). The seasonality of physically driven export at submesoscales in the northeast Atlantic Ocean. *Global Biogeochemical Cycles*, *32*, 1144–1162. https://doi.org/10.1029/2018GB005927

Estapa, M. L., Siegel, D. A., Buesseler, K. O., Stanley, R. H. R., Lomas, M. W., & Nelson, N. B. (2015). Decoupling of net community and export production on submesoscales in the Sargasso Sea. *Global Biogeochemical Cycles*, *29*, 1266–1282. https://doi.org/10.1002/2014GB004913

Falkowski, P. G., Barber, R. T., & Smetacek, V. (1998). Biogeochemical controls and feedbacks on ocean primary production. *Science*, *281*(5374), 200–206. https://doi.org/10.1126/science.281.5374.200

Giering, S. L. C., Sanders, R., Lampitt, R. S., Anderson, T. R., Tamburini, C., Boutrif, M., et al. (2014). Reconciliation of the carbon budget in the ocean's twilight zone. *Nature*, *507*(7493), 480. https://doi.org/10.1038/nature13123

Guidi, L., Calil, PauloH. R., Duhamel, S., Björkman, K. M., Doney, S. C., Jackson, G. A., et al. (2012). Does eddy-eddy interaction control surface phytoplankton distribution and carbon export in the North Pacific Subtropical Gyre? *Journal of Geophysical Research*, *117*, G02024. https://doi.org/10.1029/2012JG001984

Gula, J., Molemaker, M. J., & McWilliams, J. C. (2014). Submesoscale cold filaments in the Gulf Stream. *Journal of Physical Oceanography*, *44*(10), 2617–2643. https://doi.org/10.1175/JPO-D-14-0029.1

Hansell, D. A. (2013). Recalcitrant dissolved organic carbon fractions. *Annual Review of Marine Science*, *5*(1), 421–445. https://doi.org/10.1146/annurev-marine-120710-100757

Hansell, D. A., & Carlson, C. A. (Eds.) (2015). *Biogeochemistry of marine dissolved organic matter* (2nd ed.). Boston: Academic Press. https://doi.org/10.1016/B978-0-12-405940-5.09994-5

Hansell, D. A., Carlson, C. A., Repeta, D. J., & Schlitzer, R. (2009). Dissolved organic matter in the ocean: A controversy stimulates new insights. *Oceanography*, *22*(4), 202–211. https://darchive.mblwhoilibrary.org/handle/1912/3183

Hansen, A. N., & Visser, A. W. (2016). Carbon export by vertically migrating zooplankton: An optimal behavior model. *Limnology and Oceanography*, *61*(2), 701–710. https://doi.org/10.1002/lno.10249

Harrison, C. S., Long, M. C., Lovenduski, N. S., & Moore, J. K. (2018). Mesoscale effects on carbon export: A global perspective. *Global Biogeochemical Cycles*, *32*, 680–703. https://doi.org/10.1002/2017GB005751

Hausmann, U., McGillicuddy, D. J., & Marshall, J. (2017). Observed mesoscale eddy signatures in Southern Ocean surface mixed-layer depth. *Journal of Geophysical Research: Oceans*, *122*, 617–635. https://doi.org/10.1002/2016JC012225

Henson, S. A., Sanders, R., & Madsen, E. (2012). Global patterns in efficiency of particulate organic carbon export and transfer to the deep ocean. *Global Biogeochemical Cycles*, *26*, GB1028. https://doi.org/10.1029/2011GB004099

Henson, S. A., Sanders, R., Madsen, E., Morris, P. J., Le Moigne, F., & Quartly, G. D. (2011). A reduced estimate of the strength of the ocean's biological carbon pump. *Geophysical Research Letters*, *38*, L04606. https://doi.org/10.1029/2011GL046735

Jónasdóttir, S. H., Visser, A. W., Richardson, K., & Heath, M. R. (2015). Seasonal copepod lipid pump promotes carbon sequestration in the deep North Atlantic. *Proceedings of the National Academy of Sciences*, *112*(39), 12,122–12,126. https://doi.org/10.1073/pnas.1512110112

Karleskind, P., Lévy, M., & Memery, L. (2011). Subduction of carbon, nitrogen, and oxygen in the northeast Atlantic. *Journal of Geophysical Research*, *116*, C02025. https://doi.org/10.1029/2010JC006446

Laws, E. A., Falkowski, P. G., Smith, W. O., Ducklow, H., & McCarthy, J. J. (2000). Temperature effects on export production in the open ocean. *Global Biogeochemical Cycles*, *14*(4), 1231–1246. https://doi.org/10.1029/1999GB001229

Lévy, M., Bopp, L., Karleskind, P., Resplandy, L., Ethe, C., & Pinsard, F. (2013). Physical pathways for carbon transfers between the surface mixed layer and the ocean interior. *Global Biogeochemical Cycles*, *27*, 1001–1012. https://doi.org/10.1002/gbc.20092

Lévy, M., Ferrari, R., Franks, P. J. S., Martin, A. P., & Riviére, P. (2012). Bringing physics to life at the submesoscale: FRONTIER. *Geophysical Research Letters*, *39*, L14602. https://doi.org/10.1029/2012GL052756

Lévy, M., Iovino, D., Resplandy, L., Klein, P., Madec, G., Tréguier, A.-M., et al. (2012). Large-scale impacts of submesoscale dynamics on phytoplankton: Local and remote effects. *Ocean Modelling*, *43-44*, 77–93. https://doi.org/10.1016/j.ocemod.2011.12.003

Lévy, M., Klein, P., & Treguier, A.-M. (2001). Impact of sub-mesoscale physics on production and subduction of phytoplankton in an oligotrophic regime. *Journal of Marine Research*, *59*(4), 535–565. http://www.ingentaconnect.com/content/jmr/jmr/2001/00000059/00000004/art00003

Lévy, M., Klein, P., Tréguier, A.-M., Iovino, D., Madec, G., Masson, S., & Takahashi, K. (2010). Modifications of gyre circulation by sub-mesoscale physics. *Ocean Modelling*, *34*(1-2), 1–15. https://doi.org/10.1016/j.ocemod.2010.04.001

Lévy, M., Resplandy, L., Klein, P., Capet, X., Iovino, D., & Ethé, C. (2012). Grid degradation of submesoscale resolving ocean models: Benefits for offline passive tracer transport. *Ocean Modelling*, *48*, 1–9. https://doi.org/10.1016/j.ocemod.2012.02.004

Llort, J., Langlais, C., Matear, R., Moreau, S., Lenton, A., & Strutton Peter, G. (2018). Evaluating Southern Ocean carbon eddy-pump from biogeochemical-Argo floats. *Journal of Geophysical Research: Oceans*, *123*, 971–984. https://doi.org/10.1002/2017JC012861

Madec, G. (2008). NEMO ocean engine. Note du Póle de modélisation, Institut Pierre-Simon Laplace (IPSL), France, No 27, ISSN No 1288-1619.

Mahadevan, A. (2016). The impact of submesoscale physics on primary productivity of plankton. *Annual Review of Marine Science*, *8*(1), 161–184. https://doi.org/10.1146/annurev-marine-010814-015912

Mahadevan, A., Tagliabue, A., Bopp, L., Lenton, A., Memery, L., & Levy, M. (2011). Impact of episodic vertical fluxes on sea surface pCO_2. *Philosophical Transactions of the Royal Society A: Mathematical, Physical and Engineering Sciences*, *369*(1943), 2009–2025. https://doi.org/10.1098/rsta.2010.0340

McGillicuddy, D. J. (2016). Mechanisms of physical-biological-biogeochemical interaction at the oceanic mesoscale. *Annual Review of Marine Science*, *8*(1), 125–159. https://doi.org/10.1146/annurev-marine-010814-015606

McGillicuddy, D. J., Anderson, L. A., Bates, N. R., Bibby, T., Buesseler, K. O., Carlson, C. A., et al. (2007). Eddy/wind interactions stimulate extraordinary Mid-Ocean plankton blooms. *Science*, *316*(5827), 1021–1026. https://doi.org/10.1126/science.1136256

McWilliams, J. C. (2016). Submesoscale currents in the ocean. *Proceedings of the Royal Society A*, *472*(2189), 20160117. https://doi.org/10.1098/rspa.2016.0117

Newton, P. P., Lampitt, R. S., Jickells, T. D., King, P., & Boutle, C. (1994). Temporal and spatial variability of biogenic particles fluxes during the JGOFS northeast Atlantic process studies at 47n, 20w. *Deep Sea Research Part I: Oceanographic Research Papers*, *41*(11), 1617–1642. https://doi.org/10.1016/0967-0637(94)90065-5

Omand, M. M., D'Asaro, E. A., Lee, C. M., Perry, M. J., Briggs, N., Cetinić, I., & Mahadevan, A. (2015). Eddy-driven subduction exports particulate organic carbon from the spring bloom. *Science*, *348*(6231), 222–225. https://doi.org/10.1126/science.1260062

Resplandy, L., Lévy, M., Bopp, L., Echevin, V., Pous, S., Sarma, V. V. S. S., & Kumar, D. (2012). Controlling factors of the oxygen balance in the Arabian Sea's OMZ. *Biogeosciences*, *9*(12), 5095–5109. https://doi.org/10.5194/bg-9-5095-2012

Resplandy, L., Martin, A. P., Le Moigne, F., Martin, P., Aquilina, A., Mémery, L., et al. (2012). How does dynamical spatial variability impact 234th-derived estimates of organic export? *Deep Sea Research Part I: Oceanographic Research Papers*, *68*, 24–45. https://doi.org/10.1016/j.dsr.2012.05.015

Roshan, S., & DeVries, T. (2017). Efficient dissolved organic carbon production and export in the oligotrophic ocean. *Nature Communications*, *8*(1), 2036. https://doi.org/10.1038/s41467-017-02227-3

Schlitzer, R. (2004). Export production in the equatorial and North Pacific derived from dissolved oxygen, nutrient and carbon data. *Journal of Oceanography*, *60*(1), 53–62. http://www.springerlink.com/index/UL2015445P4TN046.pdf

Siegel, D. A., Buesseler, K. O., Doney, S. C., Sailley, S. F., Behrenfeld, M. J., & Boyd, P. W. (2014). Global assessment of ocean carbon export by combining satellite observations and food-web models. *Global Biogeochemical Cycles*, *28*, 181–196. https://doi.org/10.1002/2013GB004743

Steinberg, D. K., & Landry, M. R. (2017). Zooplankton and the ocean carbon cycle. *Annual Review of Marine Science*, *9*(1), 413–444. https://doi.org/10.1146/annurev-marine-010814-015924

Stukel, M. R., Aluwihare, L. I., Barbeau, K. A., Chekalyuk, A. M., Goericke, R., Miller, A. J., et al. (2017). Mesoscale ocean fronts enhance carbon export due to gravitational sinking and subduction. *Proceedings of the National Academy of Sciences*, *114*(6), 1252–1257. https://doi.org/10.1073/pnas.1609435114

Stukel, M. R., & Ducklow, H. W. (2017). Stirring up the biological pump: Vertical mixing and carbon export in the Southern Ocean. *Global Biogeochemical Cycles*, *31*, 1420–1434. https://doi.org/10.1002/2017GB005652

Stukel, M. R., Song, H., Goericke, R., & Miller, A. J. (2017). The role of subduction and gravitational sinking in particle export, carbon sequestration, and the remineralization length scale in the California Current Ecosystem: Subduction and sinking particle export in the CCE. *Limnology and Oceanography*, *63*(1), 363–383. https://doi.org/10.1002/lno.10636

Waite, A. M., Stemmann, L., Guidi, L., Calil, P. H. R., Hogg, A. M. C., Feng, M., et al. (2016). The wineglass effect shapes particle export to the deep ocean in mesoscale eddies. *Geophysical Research Letters*, *43*, 9791–9800. https://doi.org/10.1002/2015GL066463

Whitt, D. B., Lévy, M., & Taylor, J. R. (2017). Low-frequency and high-frequency oscillatory winds synergistically enhance nutrient entrainment and phytoplankton at fronts. *Journal of Geophysical Research: Oceans*, *122*, 1016–1041. https://doi.org/10.1002/2016JC012400